Materials Today: Proceedings xxx (xxxx) xxx

Contents lists available at ScienceDirect

Materials Today: Proceedings

journal homepage: www.elsevier.com/locate/matpr

Capability of RANS simulation to predict laminar separation bubble on the E216 airfoil

B.K. Sreejith, Vighnesha Nayak

Department of Mechanical Engineering, AJIET, Mangaluru 575006, India

ARTICLE INFO

Article history:
Received 3 March 2021
Accepted 15 March 2021
Available online xxxx

Keywords:
Airfoil
Laminar flow
Laminar separation bubble
Turbulence

ABSTRACT

Laminar separation bubble (LSB) is an aerodynamic phenomenon often observed over airfoil under low Reynolds number condition. In the present work, numerical simulation is carried out on the E216 airfoil at Reynolds number of 100,000 and various angle of attack 0°–14° to assess its aerodynamic performance. The prime motivation of the work is to predict the handling capacity of RANS turbulence model in the prediction of LSB. The Xfoil results are compared at the same working condition for the validation. The lift coefficient, *Cl* increases with increase in AOA upto maximum value of 1.46 at AOA of 12° with average deviation of 6.2% from Xfoil predictions. The drag coefficient, *Cd,* at 12° angle of attack is 0.0588 with average deviation of 5.13% from Xfoil value. Presence of pressure plateau in coefficient of pressure plot clearly depicts the formation of the LSB. The Transition RANS model could successfully predict the LSB phenomenon.

Selection and peer-review under responsibility of the scientific committee of the International Conference on Smart and Sustainable Developments in Materials, Manufacturing and Energy Engineering.

1. Introduction

Energy is basic need in day to day life. The most common form of energy is electricity. India is world's fourth largest consumer of electricity [1]. One of the major problems of today's world is limited availability of conventional energy sources. So, non-conventional energy is becoming popular because of its availability. Out of various non-conventional energy fields, wind energy field has high potential and scope of growth. Wind energy is a clean, inexhaustible and sustainable energy source. At the end of 2015, the worldwide total installed capacity of wind energy is 432883 MW in which installed capacity in India is 25088 MW (Fourth largest country). At September 2016, the installed capacity of wind power generation in India is around 28.08 GW which is 61% of total renewable energy sector [2]. NIWE has announced revised estimation of potential of wind energy is 102,788 MW at 80 m hub height [3].

In regions of low wind speed and in urban areas, small or micro wind turbines are more suitable [4]. The laminar separation and laminar separation bubbles (LSB) on the blades of small wind turbines operating at low wind speeds [5] significantly reduces its performance. The key reason is the low Reynolds number (Re) ($Re \leq 105$) [6,7] due to the small rotor size and low wind speeds. The development of optimised low Re airfoils are capable of start up at lower wind speeds with increasing the start-up torque. Thus it widens the applicability of SSWT.

Mitigating the LSB which degrades aerodynamic performance of airfoil, wind turbine blade performance can be improved. The LSB formation deteriorates aerodynamic performance of small scale wind turbine blade with increases airfoil foam drag due to induces pseudo thickness to airfoil surface [8]. M. Gaster [9] studied the effect of Re on LSB formation at different pressure distribution. The structure of the LSB significantly affected by the Re of the separating boundary layer. It is found out that laminar separation bubble is dominant in case of low Re.

In the present work numerical simulation is carried out to study the aerodynamic performance of E216 airfoil at Reynolds number of 1,00,000 and various AOA. The effectiveness of RANS transition moel in the LSB prediction is studied in the work along with the dependency of the LSB on AOA.

2. Methodology

In The E216 Airfoil is highly cambered and thin in geometry used for low Re applications like Miniature aerial vehicles and

https://doi.org/10.1016/j.matpr.2021.03.453

Selection and peer-review under responsibility of the scientific committee of the International Conference on Smart and Sustainable Developments in Materials, Manufacturing and Energy Engineering.

Please cite this article as: B.K. Sreejith and V. Nayak, Capability of RANS simulation to predict laminar separation bubble on the E216 airfoil, Materials Today: Proceedings, https://doi.org/10.1016/j.matpr.2021.03.453

the SSWT. The wind turbine power generation is directly proportional to lift to drag ratio [10]. The candidate airfoil selection is based on the highest lift to drag ratio from the set of airfoil considered for the study. The initial assessment is performed with Xfoil [11] for Re of 100,000. Fig. 1 shows the geometry of the selected airfoil. It has a maximum camber of 4.7% at x/c = 59% and a maximum thickness of 10.4% at x/c = 26.2%.

A 2D analysis is carried out with ANSYS Fluent 16.0. The geometry and meshing done with ANSYS ICEM-CFD (Fig. 2). Chord length of the aifoil is maintained as 0.15 m. The domain details are as follows: Total length = 25c to ensure fully developed flow before approaching airfoil, the width = 20c [12] to avoid wall effects. High resolution the mesh is generated in the region near to the airfoil where the study is mainly focussed with $y+$ value less than one near the airfoil surface.

The airfoil is considered as no slip surface with velocity and pressure are inlet and outlet boundary conditions respectively. Temperature is taken as 308 K with Re of 1,00,000 which corresponds to 0.15 m airfoil chord length and free stream inlet velocity of 10.08 m/s. Flow is considered as incompressible. The momentum equations are solved using semi-implicit method for pressure linked equations (SIMPLE) algorithm [13] and a second order upwind spacial discretization is considered for the calculations. For spacial gradient, least square cell based method is used. Residual value of 10–6 is set as convergence criteria.

2.1. Turbulence model

The RANS Transitional SST Model is used for the purpose of the LSB modelling [14]. It solves k – ω SST equation with two additional equations, one for intermittency (γ) and another for transitional Reynolds number ($Re_{\theta t}$) to predict the laminar-turbulent transition phenomenon. The governing equations are listed below [13–15].

The k - ω SST equation are given in Eqs. (1) and (2) with the notations have usual meaning.

$$\frac{\partial \rho k}{\partial t} + \frac{\partial \rho U_j k}{\partial x_j} = \widetilde{G_k} - Y_k + S_k + \frac{\partial}{\partial x}\left(\Gamma_k \frac{\partial k}{\partial x_j}\right) \tag{1}$$

$$\frac{\partial \rho \omega}{\partial t} + \frac{\partial \rho U_j \omega}{\partial x_j} = \widetilde{G_\omega} - Y_\omega + S_\omega + \frac{\partial}{\partial x}\left(\Gamma_\omega \frac{\partial \omega}{\partial x_j}\right) \tag{2}$$

The intermittency (γ)-transport equation is given in Eq. (3).

$$\frac{\partial \rho \gamma}{\partial t} + \frac{\partial \rho U_j \gamma}{\partial x_j} = P_{\gamma 1} - E_{\gamma 1} + P_{\gamma 2} + E_{\gamma 2} + \frac{\partial}{\partial x_j}\left[\left(\mu + \frac{\mu_t}{\sigma_t}\right)\frac{\partial \gamma}{\partial x_j}\right] \tag{3}$$

The transition source terms in the Eq. (3) are,

$$P_{\gamma 1} = 2F_{length}\rho S[\gamma F_{onset}]^{c_{\gamma 3}} \tag{4}$$

$$E_{\gamma 1} = P_{\gamma 1}\gamma \tag{5}$$

where S represents the strain rate magnitude and Flength is an empirical correlation that controls the length of the transition region. Destruction source terms are given by,

$$P_{\gamma 2} = c_{a2}\rho\Omega\gamma F_{turb} \tag{6}$$

$$E_{\gamma 2} = c_{e2}P_{\gamma 2}\gamma \tag{7}$$

here, Ω represents vorticity magnitude. The functions which control transition onset, *Fonset* are:

$$Re_v = \frac{\rho y^2 S}{\mu} \tag{8}$$

$$R_T = \frac{\rho k}{\mu \omega} \tag{9}$$

$$F_{onset1} = \frac{Re_v}{2.193 Re_{\theta c}} \tag{10}$$

$$F_{onset2} = \min\left(\max\left(F_{onset1}, F_{onset1}^4\right).2.0\right) \tag{11}$$

$$F_{onset3} = \max\left(1 - \left(\frac{R_T}{2.5}\right)^3, 0\right) \tag{12}$$

$$F_{onset} = \max\left(F_{onset2} - F_{onset3}, 0\right) \tag{13}$$

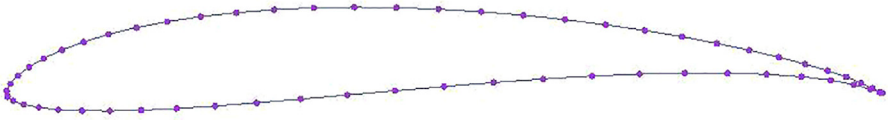

Fig. 1. E216 airfoil profile.

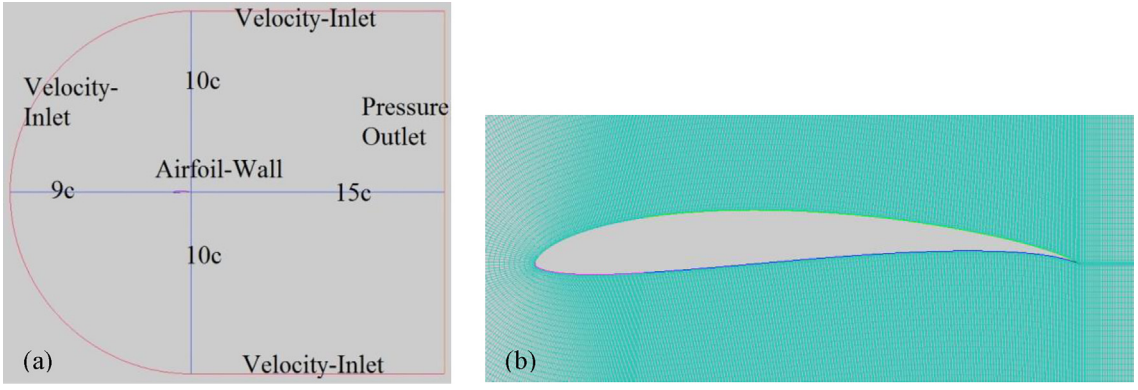

Fig. 2. (a) Computational domain and (b) Mesh around airfoil.

$$F_{turb} = e^{-\left(\frac{R_T}{4}\right)^4} \tag{14}$$

Here $Re_{\theta c}$ is the critical Re at which the intermittency starts to accumulate in the boundary layer and y is distance from wall. The $\widetilde{Re_{\theta t}}$ is the transition Re. Both the $Re_{\theta c}$ and F_{length} correlations depends on $\widetilde{Re_{\theta t}}$. The strain rate Re given by the terms Rev, k is the turbulent kinetic energy with ωas specific turbulence dissipation rate and Re_T is viscosity ratio Re. The value of constants used in the intermittancy equations are, $c\gamma 1 = 0{:}06$; $ce2 = 50$; $c\gamma 3 = 0{:}5$ and $\sigma\gamma = 1{:}0$.

The transition momentum thickness Re number, $\widetilde{Re_{\theta t}}$, is given by Eqn. (15).

$$\frac{\partial \rho \widetilde{Re_{\theta t}}}{\partial t} + \frac{\partial \rho U_j \widetilde{Re_{\theta t}}}{\partial x_j} = P_{\theta t} + \frac{\partial}{\partial x_j}\left[\sigma_{\theta t}\left(\mu + \mu_t\right)\frac{\partial \widetilde{Re_{\theta t}}}{\partial x_j}\right] \tag{15}$$

where $P_{\theta t} = c_{\theta t}\frac{\rho}{t}\left(Re_{\theta t} - \widetilde{Re_{\theta t}}\right)(1.0 - F_{\theta t})$, $t = \frac{500\mu}{\rho U^2}$ and $F\theta t$ is the blending function used to turn off the source term in the boundary layer [13–15]. Instead of the values of the constants in the equation (15), $c\theta t = 0.03$ and $\sigma\theta t = 2.0$, for reliable results, the present work used the following values in the simulations [15,16];

$c_{\theta t} = 0.02$; $\sigma_{\theta t}$=3.0.

2.2. Separation - induced transition correction

Separation-induced transition can be re written as,

$$\gamma_{sep} = mim\left[2.\max\left[\left(\frac{Re_v}{3.235Re_{\theta c}}\right) - 1, 0\right]F_{reattach}, 2\right]F_{\theta t} \tag{16}$$

$$F_{reattach} = e^{-\left(\frac{R_T}{20}\right)^4} \tag{17}$$

$$\gamma_{eff} = \max\left(\gamma_{sep}, \gamma\right) \tag{18}$$

2.3. Coupling the transition model with SST transport equations

The coulpling of transition model with the SST turbulence model is done as below:

$$\partial\rho k/\partial t + (\partial\rho U\_ik)/(\partial x\_i) = G\_k^* - Y\_k^* + S\_k + \frac{\partial}{\partial x_i}\left(\Gamma_k \frac{\partial k}{\partial x_j}\right) \tag{19}$$

$$\text{Where}, Y_k^* = \min\left(\max\left(\gamma_{eff}, 0.1\right), 1.0\right)Y_k \tag{20}$$

$$\text{And}, G_k^* = \gamma_{reff} G_k \tag{21}$$

where, Yk and Gk are the terms representing original destruction and production respectively for the SST model. The production term in the ω-equation is used without any modification.

3. Results and discussion

3.1. Grid analysis

The variation in Cl and Cd with various number of elements observed at AOA of 0^0 are used for the selection of optimum grid size. The grid number varied from 0.09 million to 0.41 million and the results are plotted in Fig. 3. The results showed that, when the number of elements crosses 3,83,060, Cl and Cd values exhibited no variation with increase in number of elements. Hence, this mesh size is being selected for further simulations.

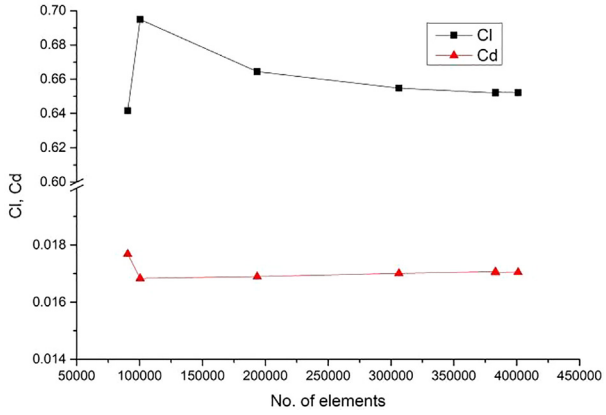

Fig. 3. Grid dependency study for AOA = 0°.

3.2. Airfoil simulation for different angle of attack

The airfoil simulations are carried out for different AOA at Reynolds number of 1,00,000 using Transition 4 equation model. For baseline simulations, lift and drag coefficient values for different AOA and their comparison with Xfoil predictions are shown in Fig. 4.

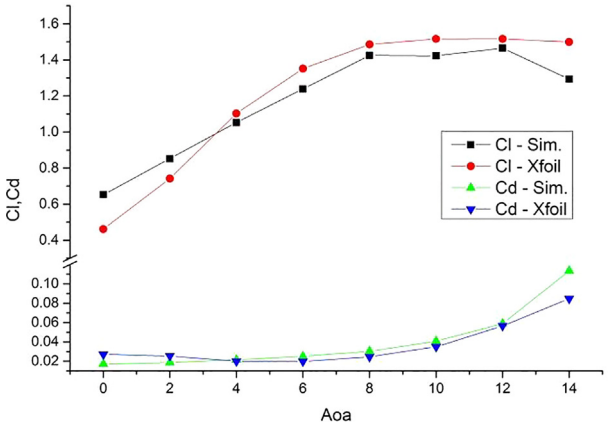

Fig. 4. Lift and drag coefficient variation with AOA.

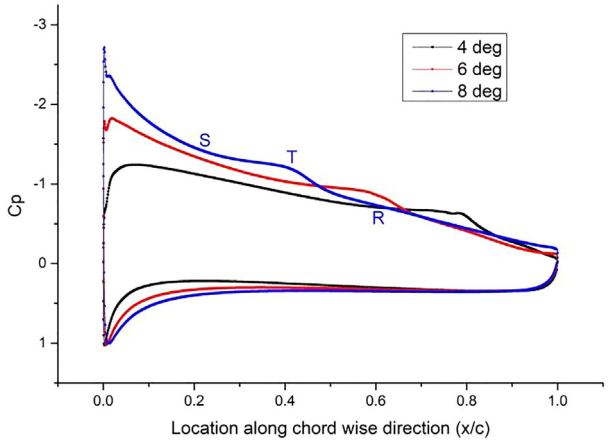

Fig. 5. Pressure coefficient over airfoil for different AOA (S – R represents LSB region).

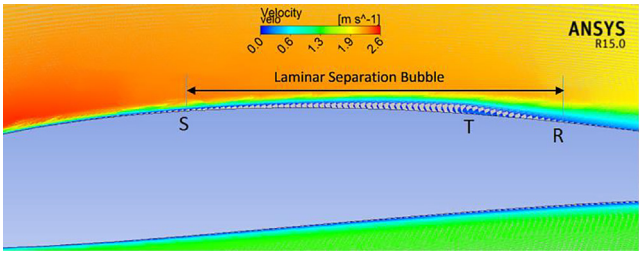

Fig. 6. Velocity profile for the airfoil showing lsb at 4° AOA.

The Cl value increases with increase in AOA upto maximum value of 1.46 at AOA of 12° with average deviation of 6.2% from Xfoil predictions. After 120, *Cl* drops because of stalling phenomena. The value of *Cd* at 12° angle of attack is 0.0588 with average deviation of 5.13% from Xfoil value. Sharp increase in *Cd* can be observed beyond 12° AOA due to stalling.

Fig. 5 shows the *Cp* distribution over the airfoil surface at various AOA. Presence of pressure plateau (line S-T) clearly depicts the formation of LSB. Point S represents separation point where flow separates from airfoil surface, point T represents transition where the detached flow mix up with upper layers of flow resulting in momentum transfer and re-energize and reattaches to airfoil surface at point R. So the region S-R represents LSB. From Fig. 5, it can be seen that location of LSB starts from 0.45c for AOA = 4°. The same can be observed in the velocity plot for the airfoil at AOA of 4° (Fig. 6).

4. Conclusion

In the present work numerical simulation of E216 airfoil is carried out at Reynolds number of 100,000 and various angle of attack 00–140 to assess its aerodynamic performance. The simulation results were validated with Xfoil predictions. Presence of pressure plateau in *Cp* plot is the indication of the formation of the LSB. The same can be observed from velocity vector plot also. As the angle of attack increased, the location of the LSB onset moved towards the leading edge of the airfoil. It indicates that the Transition RANS model could successfully predict the LSB phenomenon.

CRediT authorship contribution statement

B.K. Sreejith: Conceptualization, Methodology, Formal analysis, Investigation, Writing - original draft. **Vighnesha Nayak:** .

Declaration of Competing Interest

The authors declare that they have no known competing financial interests or personal relationships that could have appeared to influence the work reported in this paper.

References

[1]] Angelika Pullen and Steve Sawyer. Global wind report. annual market update 2015. 2016.
[2] MNRE. http://mnre.gov.in/mission-and-vision-2/achievements, 2016. Accessed: 2016-11- 07.
[3] NIW. http://niwe.res.in/department_wra_est.php, 2016. Accessed: 2016-11-06.
[4] M Ragheb. Wind turbines in the urban environment. Retrieved July, 12:2009, 2008.
[5] W.D. Musial, D.E. Cromack, Influence of reynolds number on performance modeling of horizontal axis wind rotors, J. Solar Energy Eng. 110 (2) (1988) 139–144.
[6] P.B.S. Lissaman, Low-reynolds-number airfoils, Annu. Rev. Fluid Mech. 15 (1) (1983) 223–239.
[7] W.A. Sirignano, Small wind turbines: analysis, design and application, AIAA J. 51 (8) (2013).
[8] R.K. Singh, M. Rafiuddin, Ahmed, Blade design and performance testing of a small wind turbine rotor for low wind speed applications, Renewable Energy 5 (2013) 812–819.
[9] M. Gaster, On the Stability of Parallel Flows and the Behaviour of Separation Bubbles PhD thesis, University of London, Queen Mary, 1963.
[10] James F Manwell, Jon G McGowan, Anthony L Rogers, Wind Energy Explained: Theory, Design and Application, John Wiley & Sons, 2010.
[11] Mark Drela and Harold Youngren. Xfoil 6.94 user guide, 2001.
[12] Douvi C. Eleni, Tsavalos I. Athanasios, Margaris P. Dionissios, Evaluation of the turbulence models for the simulation of the flow over a national advisory committee for aeronautics (naca) 0012 airfoil, J. Mech. Eng. Res. 4 (3) (2012) 100–111.
[13] FLUENT. 15.0. Theory Guide, 2014.
[14] F.R. Menter, R. Langtry, S V¨olker., Transition modelling for general purpose cfd codes, Flow, Turbulence Combust. 77 (1–4) (2006) 277–303.
[15] Haseeb Shah, Sathyajith Mathew, Chee Ming Lim, Numerical simulation of flow over an airfoil for small wind turbines using then gamma-*fn* text *f*Regg *fn* thetag model, Int. J. Energy Environ. Eng. 6 (4) (2015) 419–429.
[16] K.A. Fagbenro, M.A. Mohamed, D.H. Wood, Computational modeling of the aerodynamics of windmill blades at high solidity, Energy Sustain. Dev. 22 (13) (2014) 20.